Biophysical and Molecular Mechanisms of *Shaker* Potassium Channel Inactivation

TOSHINORI HOSHI, WILLIAM N. ZAGOTTA, RICHARD W. ALDRICH*

The potassium channels encoded by the *Drosophila Shaker* gene activate and inactivate rapidly when the membrane potential becomes more positive. Site-directed mutagenesis and single-channel patch-clamp recording were used to explore the molecular transitions that underlie inactivation in *Shaker* potassium channels expressed in *Xenopus* oocytes. A region near the amino terminus with an important role in inactivation has now been identified. The results suggest a model where this region forms a cytoplasmic domain that interacts with the open channel to cause inactivation.

ION CHANNELS UNDERGO CONFORMATIONAL CHANGES THAT open and close an ion-permeable pore across the membrane. In voltage-dependent channels this gating process is influenced by transmembrane voltage. *Shaker* potassium channels from *Drosophila melanogaster* open, or activate, when the membrane potential becomes sufficiently positive. After activation, the channels enter a long-lived nonconducting state, the inactivated state. A cytoplasmic domain has been implicated in this inactivation process. Single-channel experiments in native *Drosophila* muscle and in *Xenopus* oocytes injected with *Shaker* mRNA have demonstrated that the inactivation process has little intrinsic voltage dependence and that it is fast and coupled to the activation process (*1, 2*), similar to the gating of vertebrate neuronal sodium channels (*3*). The voltage-independent inactivation implies no movement of charged particles through the electric field across the membrane for the inactivation conformational change and suggests that domains that do not span the membrane are involved in inactivation. Alternatively spliced variants of the *Shaker* gene that vary only in presumed cytoplasmic domains show different inactivation kinetics when expressed in *Xenopus* oocytes (*1, 4*). Evidence from sodium channels also supports the involvement of a cytoplasmic domain in inactivation. Inactivation of sodium channels can be abolished by treating the cytoplasmic face of the channel with proteolytic enzymes (*5*), and inactivation can be mimicked by the internal application of various pharmacological agents such as guanidinium compounds (*6*).

Slowing of inactivation by trypsin. Because of the similarity in inactivation gating between *Shaker* potassium channels and sodium channels, we have investigated the effects of cytoplasmic trypsin on *Shaker* potassium channels expressed in *Xenopus* oocytes (*1, 7*). Representative records from an inside-out patch containing two channels of ShB alternatively spliced variant before and after the application of trypsin to the bath solution (Fig. 1A) show that internal trypsin treatment causes an increase in the open durations and the number of openings per burst. The effect on the decay rate of the ensemble average currents recorded with steps to +50 mV (Fig. 1B) is similar to the effects of proteolytic agents on macroscopic sodium currents (*5*). The mean duration of the openings (Fig. 1C) is increased from 0.8 ms in the control to 2.2 ms after trypsin treatment. The box plots to the right of the open duration histograms (Fig. 1C) illustrate that these effects of trypsin are reproducible. These results and the lack of effect of external trypsin on inactivation implicate the involvement of a cytoplasmic domain in inactivation.

Mutations in the amino terminal domain. We have focused on the amino terminal cytoplasmic domain because of its large number of potential trypsin sites and because of differences in inactivation gating of the channels produced by alternatively spliced amino ends (*1, 4*). To investigate the potential role of this region in inactivation, we constructed deletion mutants and examined the effects of the mutations on channel gating (*8*). The bars below the sequence in Fig. 2A show the amino acids deleted in these mutants. The interruption in the sequence after amino acid 61 shows the splice site for alternative splicing (*4*). The amino acids to the right of this site are identical in the different amino-terminal variants. The mutant ShB cDNA's were transcribed in vitro and expressed in *Xenopus* oocytes.

A representative single-channel record for each of the mutants (Fig. 2B) shows that these deletion mutations fall into two classes: (i) those that delete a portion of the sequence for the first 22 amino acids (Fig. 2A) disrupted inactivation, and (ii) those that delete amino acids on the carboxyl side of amino acid 22 leave inactivation intact. Plots of the mean open duration, the mean interburst duration, and the mean number of openings per burst for a number of single-channel patches from ShB and each of the mutations show that channels with inactivation disrupted have a longer open duration, a larger number of openings per burst, and a shorter interburst closed duration.

In the ShB cytoplasmic amino end, there are at least 61 amino acid residues (23–83) covered by the first five deletion mutations (Fig. 2A) that can be deleted without disrupting inactivation. Representative records from single-channel patches from ShB and ShBΔ23-37 (Fig. 3A) show that, although inactivation is left intact in this mutant, the rate has been altered as indicated by the decreased open durations. These decreased open durations reflect an increase in the inactivation rate rather than an increase in the rate of closing

The authors are with the Department of Molecular and Cellular Physiology, Stanford University School of Medicine, Stanford, CA 94305.

*To whom correspondence should be addressed.

to a noninactivated state. Because *Shaker* channels inactivate primarily from the open state (*2*), an increased rate of closing to a noninactivated state would produce a greater number of openings per burst and a slower rate of decay of the ensemble average at high voltages, neither of which was observed.

A quantitative comparison of the mutant channels that leave inactivation intact (Fig. 3B) shows that, although the distributions of the mean open durations for these channel species overlap, they exhibited an increasing open duration with increasing number of amino acids present in the amino-terminal region. This trend did not continue for smaller deletions or longer insertions, which showed mean open durations comparable to ShBΔ23-37 and ShB2x31-71, respectively.

To interpret our results, we have used a partial kinetic scheme derived from a more complex one developed for *Shaker* channels in *Drosophila* myotubes (*2*)

$$C \underset{\delta}{\overset{\gamma}{\rightleftharpoons}} O \underset{\lambda}{\overset{\kappa}{\rightleftharpoons}} I$$

According to this scheme, the channel closes briefly to a short-lived closed state (*C*) during a burst of openings (*O*) and closes to a long-lived inactivated state (*I*) to terminate the burst. Using this model, we have calculated the inactivation rate constant κ for each of the channel variants in Fig. 3B and plotted them as a box plot in Fig. 3C. As expected, the deletion mutants with the decreased open durations exhibit an increased rate of inactivation.

Although the last six deletion mutations shown in Fig. 2A significantly disrupt the inactivation process, they do not completely remove inactivation (Fig. 4). Although no appreciable inactivation was observed in 60 ms, most of the channels entered a long-lived inactivated state after 600 ms. The inactivation time course is similar in the channels from all of the inactivation disrupting mutants discussed thus far and in trypsin-treated channels. This slow inactivation process may not be caused by residual inactivation from the fast inactivation mechanism but may instead represent a second, fundamentally different, mechanism. A slow inactivation process was also observed in ShB channels during very long voltage pulses as indicated by exponential components with very long time constants in the closed duration histograms.

Using the kinetic model discussed above, we calculated all of the rates into and out of the open state for ShB and the deletion mutations that disrupt inactivation (Fig. 4B). None of these rates exhibited a noticeable voltage dependence over the range −20 to +50 mV, consistent with the kinetic model developed for the naturally occurring *Shaker* potassium channels (*2, 9*). The inactivation rate (κ) is significantly smaller in these deletion mutations than in ShB and the rate of return from inactivation (λ) is significantly greater. The rates into and out of the closed state (γ and δ) are not significantly altered by these deletion mutations. These data suggest that the deletion mutations that disrupt inactivation destabilize the inactivated state by approximately 3 kcal/mol and increase the energy of the transition state by 1.5 kcal/mol (*2*). In contrast to the deletions that altered the inactivation rate by an amount related to the length of the deletion (Fig. 3), these deletion mutations that disrupt inactivation show no relation between length and inactivation rate. This supports the idea that the slow, residual inactivation remaining in these mutants occurs by a separate process.

In addition to inactivation from the open state, *Shaker* channels can inactivate without opening. This closed-state inactivation can be seen in single-channel recordings as records without openings during the voltage steps (*2*). Deletion mutations that disrupt inactivation from the open state also disrupt inactivation from the closed states. Mutant channels with disrupted inactivation usually exhibited fewer records without openings than wild-type channels. Although we have not investigated this extensively, these results imply a common mechanism for inactivation from open and closed states.

Deletions that remove positive charges. Our results have shown that a deletion mutation in the amino-terminal variable region of ShB causes either faster or slower inactivation, depending on the

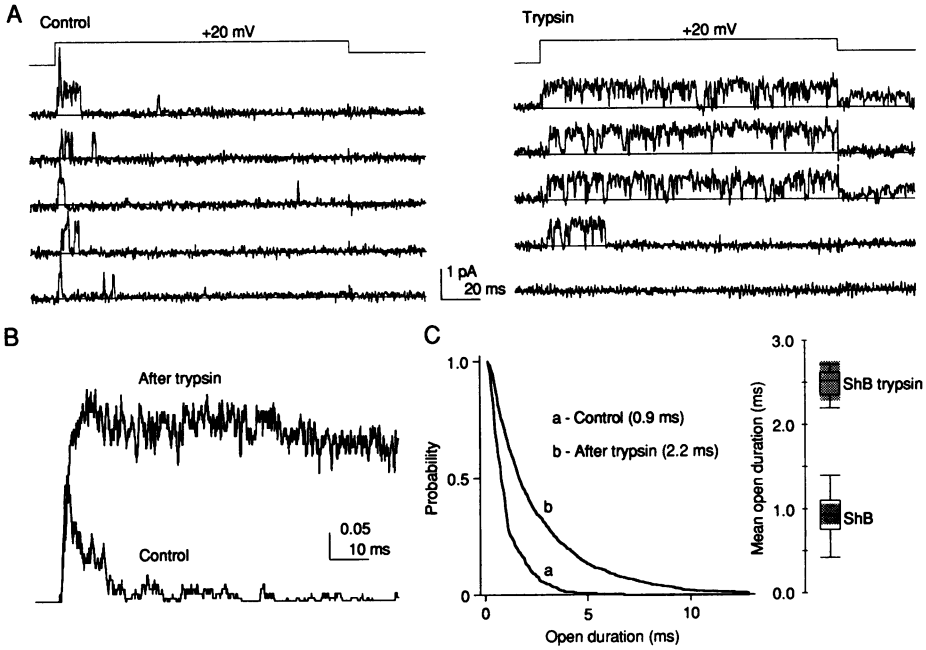

Fig. 1. Effects of intracellular trypsin on the ShB channels expressed in *Xenopus* oocytes. (**A**) Representative openings of ShB channels before and after treatment with 0.0025 percent trypsin. The channels were recorded from an inside-out patch containing two ShB channels with voltage steps to +20 mV after 1-s prepulses to −100 mV from a holding voltage of −70 mV. The data were filtered at 1 kHz and digitized at 50 μs per point. Trypsin was applied to the bath solution and remained in the bath, and the voltage pulses were applied until the effect was seen (typically 15 to 30 s) and then washed out with trypsin-free solution. Frequently the treatment with trypsin caused functional loss of one or more of the channels as in the examples shown here. Upward transitions are the opening transitions. (**B**) Ensemble averages of the ShB channels before and after trypsin. The pulse protocols are the same as in (A). The vertical scale bar is expressed in terms of probability. (**C**) Open durations of the ShB channels before and after treatment with trypsin. The open duration histograms are displayed as tail distributions and show the probability that a given open duration is greater than the time indicated on the abscissa. The mean open durations for ShB channels from a number of patches are displayed in the form of a box plot before and after trypsin treatment to the right of the distributions. The central outlined box shows the middle half of the data, approximately between the 25th and 75th percentiles. The horizontal line in the middle of the box marks the median of the data. The "whiskers" extending from the top and bottom of the box show the main body of the data. Outliers or extreme values, if present, are plotted individually with circles or stars. The shaded region illustrates the 95% confidence interval of the median (*17*). Since the mean open durations of both the control and trypsin-treated ShB channels were voltage-independent, the data obtained at different voltages (>−20 mV and <=+50 mV) were pooled.

region in which the deletion occurs. The amino acid sequence of the region where mutations disrupt inactivation contains 11 hydrophobic residues or uncharged residues followed by a highly charged region (residues 12 to 19). To investigate the potential role of the charged residues in inactivation, we constructed deletions beginning at residue 30 and extending for variable distances toward the amino terminus. The amino acid sequence of each of the mutants is shown below a family of macroscopic currents from the mutant in Fig. 5A. A deletion from residue 22 to residue 30 produces little, if any, effect on the macroscopic currents. A deletion from residue 17 to residue 30, removing three positively charged residues (two lysines and one arginine), slowed macroscopic inactivation, and a deletion of one more charged amino acid (histidine) slowed inactivation even further. The macroscopic inactivation rate of both of these mutants is intermediate between ShB and the slow inactivation of the mutants that disrupt inactivation (Figs. 2 and 3), as shown for ShBΔ6-60 (Fig. 5). The mutant ShBΔ22-30 deletes four of six consecutive glutamines (Q) without producing a significant effect on the inactivation rate, indicating that these glutamines do not play an important role in this inactivation process. The boundary between the regions where deletions show or speed up inactivation is, therefore, likely to be at the beginning of the stretch of consecutive glutamines.

These intermediate macroscopic inactivation rates correspond to intermediate single-channel inactivation transition rates (Fig. 5, B and C). The mean open and burst durations get progressively longer

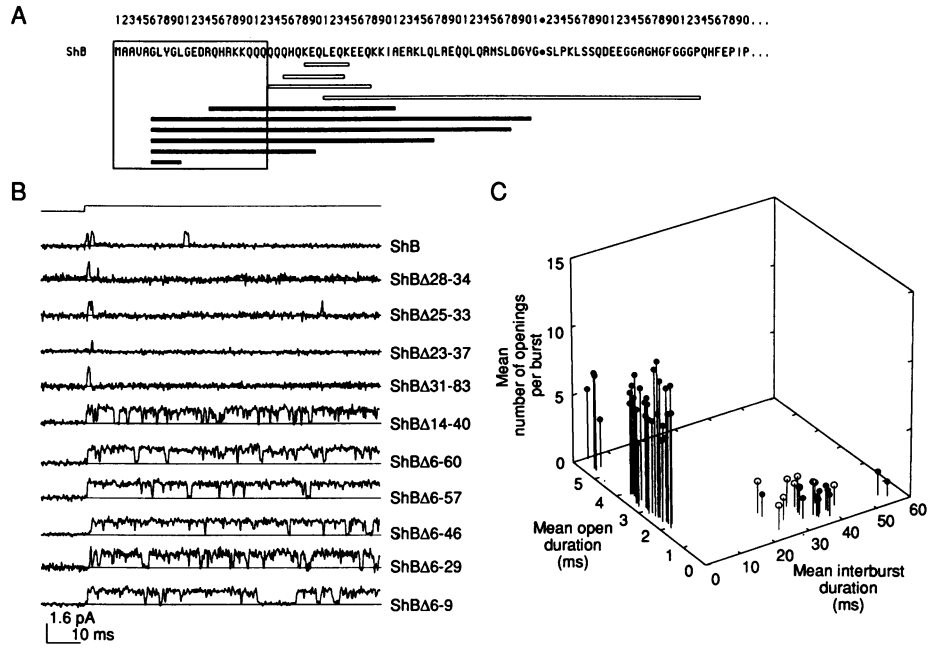

Fig. 2. (**A**) Deletion mutations in the amino-terminal variable region of ShB. The deduced sequence of the first 90 amino acids of ShB is shown at the top and the horizontal bars below indicate the deletions made. The deletions that disrupted inactivation are shown by solid bars and those that leave inactivation intact are shown by open bars. The "•" symbol in the sequence marks the position where alternatively spliced amino-terminal variants begin to diverge. (**B**) Representative single-channel openings from ShB and the deletion mutants shown in (A). The openings were elicited by a voltage step to +50 mV after a 1-s prepulse to −100 mV from a holding voltage of ≤70 mV. The data were filtered at 1.4 to 2.0 kHz and digitized at 50 μs per point. The voltage protocol is shown at the top. (**C**) Three-dimensional plot showing the relation among the mean number of openings per burst, mean open duration, and the mean interburst duration. A burst was defined as openings separated by closures of less than 1.0 or 1.2 ms, approximately three times longer than the time constant of the fastest exponential component in the closed durations. Open symbols and filled symbols represent ShB and the deletion mutants shown in (A), respectively. Abbreviations for the amino acid residues are: A, Ala; C, Cys; D, Asp; E, Glu; F, Phe; G, Gly; H, His; I, Ile; K, Lys; L, Leu; M, Met; N, Asn; P, Pro; Q, Gln; R, Arg; S, Ser; T, Thr; V, Val; W, Trp; and Y, Tyr.

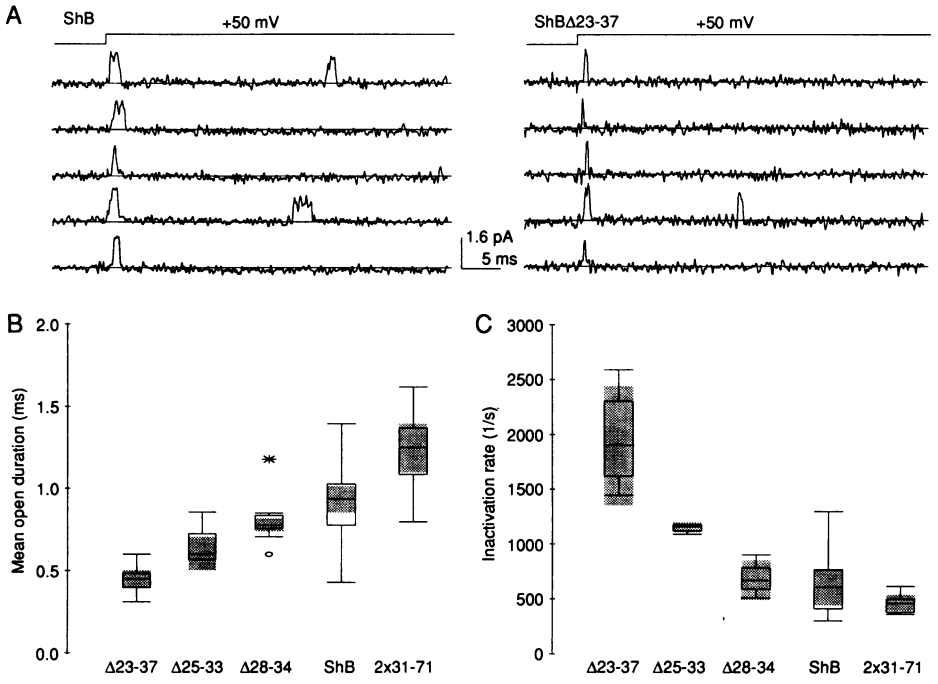

Fig. 3. Effects of the deletion mutations that did not disrupt inactivation. (**A**) Representative single-channel openings from ShB (left) and ShBΔ23-37 (right). The openings were elicited by a voltage step to +50 mV following a 1-s prepulse to −100 mV from a holding voltage of −70 mV. The data were filtered at 2 kHz and digitized at 50 μs per point. The voltage protocols are shown at the top. (**B**) Mean open durations from the mutants that alter inactivation but do not totally disrupt it. ShB2x31-71 is an insertion mutant, which contains a tandem duplication of residues 31 to 71 of the ShB sequence. The mutants are arranged on the abscissa in increasing length of the amino end, with deletions of 15, 9, 7, and 0 amino acids, and an insertion of 41 amino acids. (**C**) Inactivation rates of the mutants shown in (B). The values are calculated as [(mean number of openings per burst) × (mean open duration)]$^{-1}$.

as the deletions remove more and more of the positive charge in this region. This indicates that the inactivation transition rate becomes progressively smaller with decreasing positive charge.

Point mutations in the amino-terminal domain. To directly test the role of charged residues in this region (residues 12 to 20), we constructed a series of single and double point mutations and examined their effects on inactivation (*10*) (Fig. 6A). Neutralization of a negatively charged aspartate at position 13 (ShB-D13N) or a single positively charged lysine at position 18 along with the addition of a positive charge at position 30 (ShB-K18Q:Q30K) did not noticeably alter the macroscopic current. Furthermore, substitution of a positively charged arginine for a positively charged lysine at position 19 (ShB-K19R) produced little effect. However, neutralization of the lysines at positions 18 and 19 (ShB-K18Q:K19Q) slowed the macroscopic inactivation to a rate intermediate between ShB and the deletion mutation ShBΔ17-30, which deletes these two lysines and the neighboring arginine at position 17 (see Fig. 5). Neutralizing the two arginine residues at positions 14 and 17 (ShB-R14Q:R17Q) also slowed macroscopic inactivation. These results demonstrate the importance of these positively charged residues in the inactivation process.

To examine the effects of the point mutations that partially disrupt inactivation, we recorded single-channel currents from the mutant channels and analyzed them according to the model discussed earlier. The slower macroscopic inactivation in ShB-K18Q:K19Q is not the result of a greater open duration or burst duration, but of a greater number of bursts per depolarizing epoch (Fig. 6B, box plots). As in the case of the deletion mutations that disrupt inactivation, the increased number of bursts per depolarizing epoch indicates a faster rate of return from inactivation. However, unlike the deletion mutations, the mean open duration and mean burst duration are unaffected, indicating that the rate of entering the inactivated state is unchanged. Taken together, these results suggest that the neutralization of these charges destabilizes the inactivated state relative to the open state but leaves the transition state between these unaffected. By contrast, neutralization of the positively charged residues at positions 14 and 17 (ShB-R14Q:R17Q) causes an increase in the mean burst duration and a decrease in the interburst interval, signifying a change in both the energy of the inactivated state and the transition state.

Since the deletion mutant ShBΔ6-9 has not had any charged residues deleted and still disrupts inactivation, it is evident that inactivation requires more than just this positively charged region. The conservation of hydrophobic character in the first ten amino acids of the *Shaker* amino-terminal variants suggests that the hydrophobic nature of this region is important for inactivation. We replaced the leucine at position 7 with an arginine (positively charged), glutamate (negatively charged), or glutamine (polar) residue (ShB-L7R, ShB-L7E, ShB-L7Q). The macroscopic currents and box plots of the mean open durations (Fig. 7) indicate that charged residues at this position significantly disrupt inactivation in a manner similar to the deletion mutants of Fig. 2. A glutamine at this position exhibits a less extreme effect, as indicated by the small residual macroscopic inactivation and the shorter mean open duration in ShB-L7Q. Hydrophobic character of these amino acids appears to be important for normal inactivation.

Functional domains in the amino terminus. The first 83 amino acids of the ShB protein can be divided into two functional domains on the basis of the effects of deletions. Mutations in the first domain, constituting approximately the first 19 residues, cause a significant slowing or complete removal of the fast inactivation process of the channels. The second domain begins at about residue 20 and extends to at least residue 83; deletions in this domain speed up inactivation and insertions slow it. Deletions that extend across both domains, such as ShBΔ6-60, affect channel gating in a manner similar to the mutation in just the first domain, such as ShBΔ6-9, indicating that the disruption of inactivation overrides its enhancement by deletions in the second domain.

The effect of intracellular trypsin is similar to that of the deletion mutations in the amino-terminal variable region that disrupt inactivation. Both alterations are characterized by slowing, but not complete removal, of the inactivation process, as indicated by an increase in the open durations and number of openings per burst. When considered together with the frequent occurrence of trypsin sites in the amino-terminal end, these results suggest that trypsin exerts its action by cleaving at one or more of these sites. Since extracellular trypsin does not produce the effect, this provides support for the proposed membrane topology placing the amino terminus on the cytoplasmic side of the membrane. The similar action of intracellular trypsin on sodium channels and potassium channels may indicate a conserved mechanism of inactivation among channels with different selectivities.

Because of the finding that inactivation of sodium channels is voltage-independent (*3*), removed by proteolytic agents (*5*), and

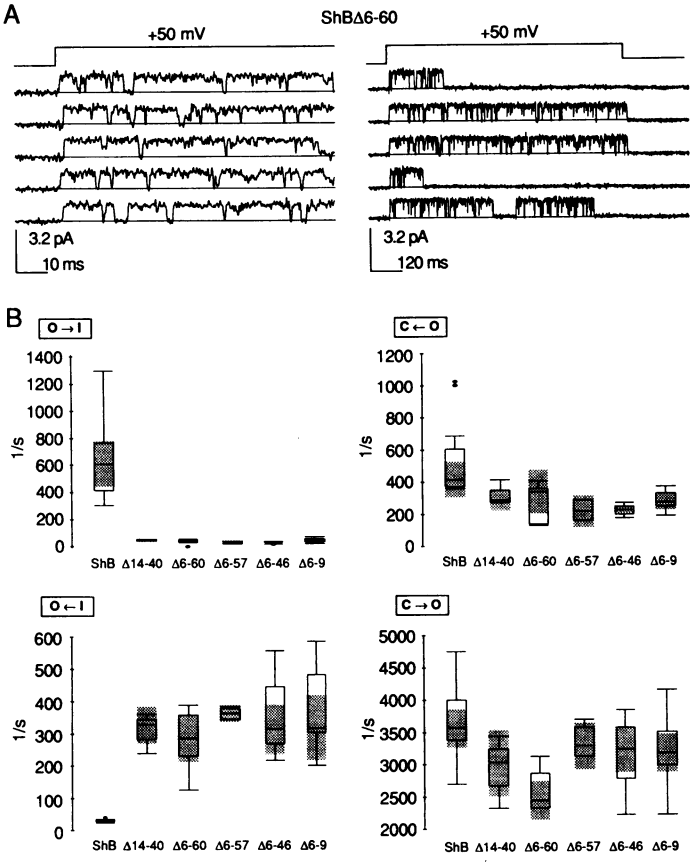

Fig. 4. (**A**) Representative openings from a mutant ShB channel (Δ6-60) recorded at +50 mV on two different time scales. The openings were elicited at +50 mV from the holding voltage of −70 mV after a 1-s prepulse to −100 mV. The records on the left were filtered at 1.8 kHz and digitized at 50 μs per point and those on the right were filtered at 800 Hz and digitized at 300 μs per point. The pulses were applied every 6 s on the left and 10 s on the right. (**B**) Box plots of the four rate constants in the closed-open-inactivated model for the deletion mutants examined. $C \rightarrow O$ values are calculated as (mean intraburst closed duration)$^{-1}$. $C \leftarrow O$ values are calculated as [mean number of openings/burst − 1]/[(mean number of openings/burst) × (mean open duration)]. $O \rightarrow I$ values are calculated as [(mean number of openings/burst) × (mean open duration)]$^{-1}$. $C \leftarrow I$ values are calculated as [mean interburst duration]$^{-1}$.

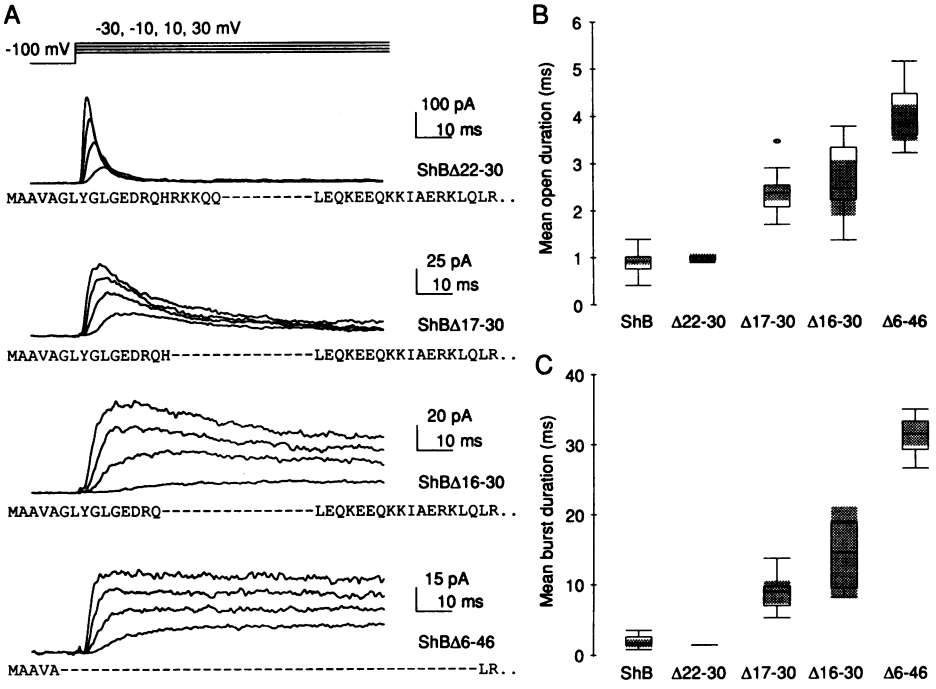

Fig. 5. Effects of the deletion mutations that remove positive charges. (**A**) Macroscopic currents obtained from the mutant channels. "–" indicates the amino acid deleted. Data from the mutation ShBΔ6-60 are shown at the bottom for reference. The macroscopic currents were from inside-out patches containing a large number of channels and were elicited with voltage steps to −30, −10, +10, and +30 mV. The data were filtered at 1.3 kHz and digitized at 100 μs per point. (**B**) Box plots of mean open durations from ShB and the mutants shown in (A). (**C**) Box plots of mean burst durations from ShB and the mutants shown in (A).

mimicked by internal perfusion with various pharmacological agents (*6*), Armstrong and Bezanilla (*11*) proposed a physical model for the inactivation of sodium channels. In this model the channel protein was proposed to have a structure similar to a ball and chain on its cytoplasmic face. Inactivation occurs in the model by the movement of the ball into the channel mouth after the channel opens. The binding site or receptacle for the ball is not available until the channel is open, or about to open, producing a coupling of activation and inactivation processes.

The "ball and chain" model for inactivation is entirely consistent with results from our experiments on ShB channels and provides a framework for interpreting the results. Like that of the sodium channels, inactivation of the *Shaker* channels is voltage-independent, partially coupled to activation, and disrupted by proteolytic enzymes. Inactivation is influenced by mutations in the first 19 amino acids, characterized by 11 consecutive hydrophobic or uncharged residues followed by 8 hydrophilic residues, including four positively charged amino acids. This region is a good candidate for the inactivation ball. Its structure of a positively charged region next to a hydrophobic region is reminiscent of tetraethyl ammonium (TEA) derivatives (*12*) and the arginine side chain *N*-propylguanidinium that mimic inactivation in potassium and sodium channels (*6*) and have been proposed to be analogs of the inactivation ball. For both of these agents the importance of both a hydrophobic and electrostatic interaction has been shown. By analogy the hydrophobic residues in the inactivation ball may interact directly with the channel. Alternatively, the hydrophobic residues may form the core of a globular domain, protected from the water environment by the charged and other hydrophilic residues. Disruption of inactivation by the mutation ShBΔ6-9 and the point mutations ShB-L7E and ShB-L7R could then be interpreted as disturbing the structure of the core of the ball, while the inactivation rates altered by the mutations ShBΔ16-30 and ShBΔ17-30 and the point mutation ShB-K18Q:K19Q could be interpreted as disrupting the positively charged character of the ball.

These first 19 residues are followed by an extended sequence of hydrophilic residues. The hydrophilic nature of this region and its large number of potential trypsin sites makes it a good candidate for the chain domain. Moreover, large deletions restricted to this region speed up inactivation, as might be expected for a mutation that shortened the chain, and insertions slow inactivation consistent with a longer chain.

The alternative splicing of various amino ends onto the core

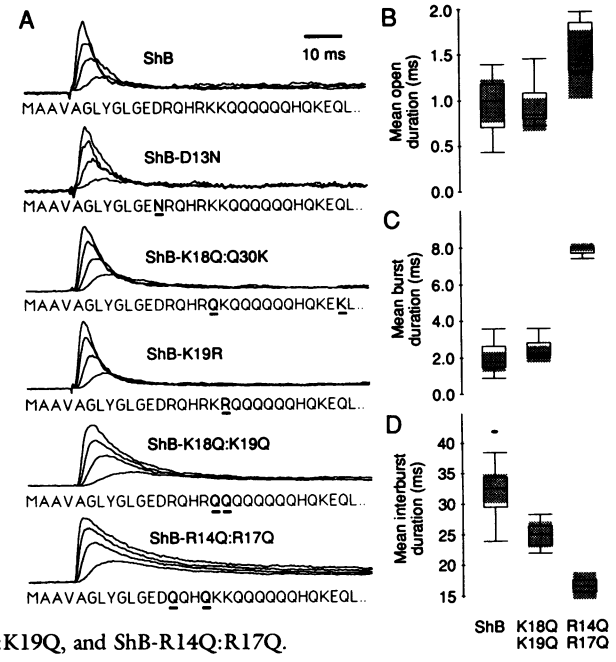

Fig. 6. (**A**) Macroscopic currents from ShB and point mutants in the hydrophilic region. Macroscopic currents were recorded at −30, −10, +10, and +30 mV. The mutated amino acids are indicated by the bold letters and underlined. The currents were recorded from inside-out patches after a 1-s prepulse to −100 mV from the holding voltage of ≤−70 mV. The data were filtered at 1.3 kHz and digitized 100 μs per point. The pulses were applied every 6 s. The records are scaled so that the peak amplitudes of the currents recorded at +50 mV are approximately the same. (**B**) Box plots of mean open durations from ShB, ShB-K18Q:K19Q, and ShB-R14Q:R17Q. (**C**) Box plots of mean burst durations from ShB, ShB-K18Q:K19Q, and ShB-R14Q:R17Q. (**D**) Box plots of mean interburst durations from ShB, ShB-K18Q:K19Q, and ShB-R14Q:R17Q.

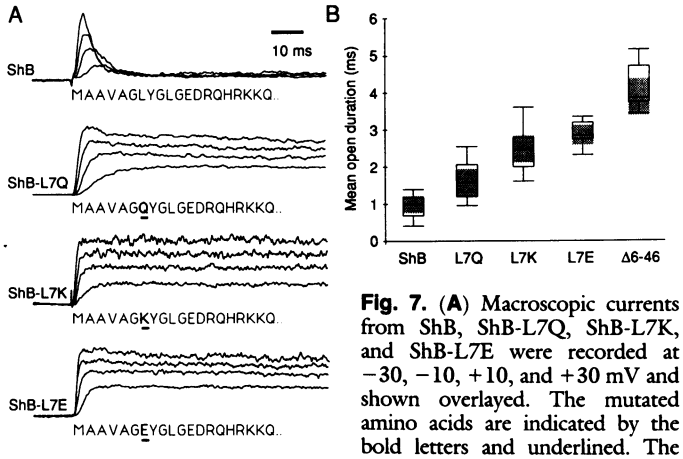

Fig. 7. (**A**) Macroscopic currents from ShB, ShB-L7Q, ShB-L7K, and ShB-L7E were recorded at −30, −10, +10, and +30 mV and shown overlayed. The mutated amino acids are indicated by the bold letters and underlined. The currents were recorded from inside-out patches after a 1-s prepulse to −100 mV from the holding voltage of ≤−70 mV. The data were filtered at 1.3 kHz and digitized 100 μs per point. The pulses were applied every 6 s. The records are scaled so that the peak amplitudes of the currents recorded at +50 mV are approximately the same. (**B**) Box plots of mean open durations from ShB, three mutants, and ShBΔ6-46.

region provides a method for generating channel variants with diverse inactivation kinetics (*13*). All of the amino variants support inactivation, but with different rates (*1, 4*). The basic plan of ten or more hydrophobic or uncharged residues followed by charged residues is repeated in all of the amino variants. If the amino end represents a ball and chain domain, then the amino acid sequences in these variants form balls with different affinities for their receptor and chains with different lengths.

The cytoplasmic region of the sodium channel between homology units III and IV is involved in inactivation (*14, 15*). Polyclonal antibodies to the region alter the inactivation rate of the channels when applied from the intracellular side (*14*). Deletion mutations and cuts in the peptide backbone in this region slow the macroscopic inactivation rate and increase the open durations (*15*). Although this region of the sodium channel shows little sequence homology to the amino-terminal region of ShB, it shares the motif of clustered positively charged residues. On the basis of these similarities in the primary structure and the effects of mutations, it seems possible that the amino-terminal region of ShB and the linkage between units III and IV in the sodium channel may be functionally homologous.

On the basis of sequence similarity with the *Shaker* channel, clones have been isolated for structural components of delayed rectifier channels from mouse and rat brain (*16*). Although these proteins are similar to the *Shaker* proteins in the putative transmembrane regions, they diverge in the amino-terminal and carboxyl-terminal regions. When expressed in *Xenopus* oocytes, most of these mammalian homologs exhibit gating similar to that of the *Shaker* mutants that disrupt inactivation, with only very slow inactivation. The rate of this slow inactivation, however, differs among the different clones, suggesting that one or more of their structural differences affect the slow inactivation rate. The slow recovery from inactivation seen in the carboxyl-terminal variants of *Shaker* may be associated with this slower inactivation process.

The ball and chain mechanism for inactivation predicts that another region of the channel will form a receptor for the inactivation ball. Mutations in the receptor region would also be expected to have effects on inactivation gating. Our results suggest that this receptor will contain both negatively charged and hydrophobic regions. It is quite possible that the amino acids from noncontiguous parts of the primary sequence form the receptor, reflecting the tertiary structure of the channel at the internal face of the membrane. Although further studies are necessary to determine the location of the receptor, a reasonable candidate is the internal mouth of the channel.

REFERENCES AND NOTES

1. W. N. Zagotta *et al.*, *Proc. Natl. Acad. Sci. U.S.A.* **86**, 7243 (1989).
2. W. N. Zagotta and R. W. Aldrich, *J. Gen. Physiol.* **95**, 29 (1990).
3. R. W. Aldrich, D. P. Corey, C. F. Stevens, *Nature* **306**, 436 (1983); R. W. Aldrich, and C. F. Stevens, *J. Neurosci.* **7**, 418 (1987); T. Gonoi and B. Hille, *J. Gen. Physiol.* **89**, 253 (1987); G. E. Kirsch and A. M. Brown, *ibid.* **93**, 85 (1989); B. A. Barres, L. L. Y. Chun, D. P. Corey, *Neuron* **2**, 1375 (1988).
4. L. C. Timpe *et al.*, *Nature* **331**, 143 (1988); L. C. Timpe *et al.*, *Neuron* **1**, 659 (1988); L. E. Iverson *et al.*, *Proc. Natl. Acad. Sci. U.S.A.* **85**, 5723 (1988).
5. C. M. Armstrong, F. Bezanilla, E. Rojas, *J. Gen. Physiol.* **62**, 375 (1973); E. Rojas and B. Rudy, *J. Physiol. (London)* **262**, 501 (1976); R. J. Stimers, F. Bezanilla, R. E. Taylor, *J. Gen. Physiol.* **85**, 65 (1985).
6. J. Z. Yeh and T. Narahashi, *Biophys. J.* **15**, 263 (1975); G. E. Kirsch *et al.*, *J. Gen. Physiol.* **76**, 315 (1980); R. Morello *et al.*, *Biophys. J.* **31**, 435 (1980); E. Rojas and M. Luxoro, *Nature* **199**, 78 (1963).
7. RNA was transcribed from cDNA, and injected into *Xenopus laevis* oocytes as described in (*1*). Patch-clamp recordings were made as in (*1*). The internal solution contained 140 mM KCl, 2 mM $MgCl_2$, 1 mM $CaCl_2$, 11 mM EGTA, and 10 mM Hepes, pH 7.2. The external solution contained 140 mM NaCl, 6 mM $MgCl_2$, and 5 mM Hepes, pH 7.1. Macroscopic currents were obtained in the inside-out configuration by using pipettes with initial resistances <1 Mohm, and no series resistance compensation was made. Recordings were made at 19° to 21°C. Data were acquired and analyzed as in (*1, 2*). Most of the single-channel data were obtained in cell-free configurations.
8. The ShBΔ6-9 deletion was generated by excising an Nae I–Sfi I fragment from the ShB construct, and the ShBΔ31-83 deletion was generated by excising an Xho I–Rsr II fragment. The deletion mutants ShBΔ6-60, ShBΔ6-57, ShBΔ6-46, and ShBΔ6-29 were prepared by a modification of the procedure for the Erase-a-Base System (Promega, Madison, WI). The pSP72 plasmid (Promega, Madison, WI) containing the ShB cDNA insert was linearized with Sfi I and digested with S1 nuclease. Deletions were generated by digesting the linearized plasmid with Exo III for 30 seconds to 2 minutes at 32°C (30 seconds at 24°C for ShBΔ6-29). The ends of the digested plasmids were made blunt by treatment with S1 nuclease and then with DNA polymerase I (Klenow fragment). The deleted *Shaker* 3′ ends were ligated to a Hind III–Nae I fragment from the ShB plasmid. The mutants ShBΔ28-34, ShBΔ25-33, ShBΔ23-37, and ShBΔ14-40 were prepared by generating bidirectional deletions from the Xho I site in ShB with Exo III. For ShBΔ22-30, ShBΔ17-30, and ShBΔ16-30, the plasmids were linearized with Xho I, and for the insertion mutation, ShB2x31-71, the plasmid was linearized with Sal I. Deletions were generated by digesting the linearized plasmids with Exo III for 30 seconds to 2 minutes at 16°C for the deletions and 30 seconds to 75 seconds at 35°C for the insertion. The deleted *Shaker* 5′ ends were then ligated to a Xho I–Bgl II fragment from the ShB plasmid. For all of the mutations, single isolates were selected and sequenced to determine the length of the deletion or insertion and to ensure that they were in the correct reading frame.
9. Since the parameters are voltage-independent (>−20 mV and <=+50 mV), data from different voltages were pooled and analyzed.
10. Point mutations were generated as described [A. R. Oliphant, A. L. Nussbaum, K. Struhl, *Gene* **44**, 177 (1986)]. Briefly, degenerate oligonucleotides were synthesized with a sequence that extends between two restriction sites in the ShB cDNA and contains the required base changes. The oligonucleotides were then made double-stranded by the method of mutually primed synthesis and cleaved with the enzyme recognizing the restriction site on the 5′ end. The dimerized, double-stranded oligonucleotide was gel-purified on a nondenaturing polyacrylamide gel and cleaved with the enzyme recognizing the internal restriction site to produce the final product, a double-stranded oligonucleotide mixture with 5′ and 3′ ends suitable for ligation. This cassette was then ligated into the *Shaker* insert cut with the same two restriction enzymes.
11. C. M. Armstrong and F. Bezanilla, *J. Gen. Physiol.* **70**, 567 (1977).
12. C. M. Armstrong, *ibid.* **58**, 413 (1971).
13. T. L. Schwarz, B. L. Tempel, D. M. Papazian, Y. N. Jan, L. Y. Jan, *Nature* **331**, 137 (1988); A. Kamb, J. Tseng-Crank, M. A. Tanouye, *Neuron* **1**, 421 (1988); O. Pongs *et al.*, *EMBO J.* **7**, 1087 (1988).
14. P. M. Vassilev, T. Scheuer, W. A. Catterall, *Science* **241**, 1658 (1988).
15. W. Stühmer *et al.*, *Nature* **339**, 597 (1989).
16. B. L. Tempel, Y. N. Jan, L. Y. Jan, *ibid.* **332**, 837 (1988); A. Baumann, A. Grupe, A. Ackermann, O. Pongs, *EMBO J.* **7**, 2457 (1988); M. J. Christie, J. P. Adelman, J. Douglass, R. A. North, *Science* **244**, 221 (1989); G. Koren *et al.*, *Neuron* **2**, 39 (1990); W. Stümer *et al.*, *EMBO J.* **8**, 3235 (1989).
17. J. W. Tukey, *Exploratory Data Analysis* (Addison-Wesley, Reading, MA, 1977); P. F. Velleman and D. C. Hoaglin, *Applications, Basics, and Computing of Exploratory Data Analysis* (Duxbury, Boston, MA, 1981).

18. We thank L. Y. Jan and Y. N. Jan for *Shaker* cDNA clones and D. Baylor, R. W. Tsien, and A. Welcher for helpful discussions. Supported by NIH grants NS23294 and NS07158, and an American Heart Association California Affiliate postdoctoral fellowship (T. H.).

11 July 1990; accepted 20 September 1990